AD-A106 350 DAVID W TAYLOR NAVAL SHIP RESEARCH AND DEVELOPMENT CE--ETC F/G 20/4
LIFTING-SURFACE HYDRODYNAMICS FOR DESIGN OF ROTATING BLADES.(U)
OCT 81 T E BROCKETT
UNCLASSIFIED DTNSRDC-81/081 NL

1 OF 1
AD
A106350

END
DATE
FILMED
11-81
DTIC

AD A106350

REPORT DOCUMENTATION PAGE

DD 1473

... continued

... geometric variables and induced velocities, ... existing techniques. ... orthogonal ... blade surface, as defined in the ... the blade is derived from the ... integral ... experimental ... efficient ...

TABLE OF CONTENTS

LIST OF FIGURES

LIST OF TABLES

THE SOCIETY OF NAVAL ARCHITECTS AND MARINE ENGINEERS
One World Trade Center, Suite 1369, New York, N.Y. 10048

Lifting-Surface Hydrodynamics for Design of Rotating Blades

No. 20

Terry Brockett, David Taylor Naval Ship Research and Development Center, Bethesda, MD

ABSTRACT

[illegible] presented for the [illegible] lifting surfaces [illegible] are [illegible]. In addition [illegible] determined from [illegible] appropriate [illegible] additional [illegible] integral [illegible] orthogonal [illegible] surface as defined [illegible] on the blades [illegible] of a singular integral [illegible] integral is used. The predictions [illegible] experimental data. A new term [illegible] arises from a radial inflow component [illegible] example illustrates the importance [illegible] design [illegible] obtained for [illegible] 400 [illegible] on the Burroughs [illegible]

NOTATION

Symbol	Definition
[illegible]	[illegible]
	Blade section drag coefficient
[illegible]	Pressure coefficient
[illegible]	Power loading coefficient based on reference speed
[illegible]	Thrust loading coefficient based on reference speed
[illegible]	Blade section chord length
[illegible]	Rotor diameter
[illegible]	Friction drag on blade section
[illegible]	Profile shape function
[illegible]	Meanline shape function
[illegible]	Thickness shape function
[illegible]	Unit base vectors in a helical reference system
[illegible]	Induction factor
[illegible]	Non-dimensional circulation
[illegible]	Total rake, axial displacement of blade section midchord point from $x = 0$ plane
[illegible] e_r, e_θ	Unit base vectors in a cylindrical polar reference system
[illegible]	Unit base vectors in a Cartesian reference frame
J_V [illegible]	Advance coefficient based on reference speed
[illegible]	Vector normal to blade surface pointing into fluid
N_R [illegible]	Radial component of N
[illegible]	Normal to blade reference surface ($\theta = 0$ surface)
[illegible]	Unit vector normal to blade surface, pointing into fluid
[illegible]	Propeller rotational speed, revolutions per unit time
[illegible]	Pressure
[illegible]	Pitch of blade section
Q	Torque absorbed by blades
[illegible]	Velocity vector
[illegible]	Velocity vector far upstream
R [illegible]	Rotor tip radius
r_h	Radius of rotor hub
[illegible]	Position vector of field point
[illegible]	Position vector of field point on blade reference surface
[illegible]	Position vector of point on k^{th} blade surface
[illegible]	Position vector of point on blade reference surface $\theta_k = 0$
[illegible]	Position vector of point on shed vortex sheet
T	Thrust produced by blades
t	Thickness of blade section
V	Reference speed
v	Velocity component due to presence of the blades
$v = (u, v, w)$	Average perturbation velocity along blade surface, due to presence of the blades
[illegible]	Velocity difference across blade surface
v_1	Even perturbation velocity component due to blade loading and shed vortex sheet

v_T	Even perturbation velocity component due to thickness
$\vec{w}$	Velocity induced by vortex filament
$w_x(x_R)$	Local wake fraction
$w_R(x_R)$	Radial free stream velocity component, fraction of V
(x, y, z)	Cartesian coordinates
x	Cartesian coordinate for field point on blade surface
x_c	Fraction of chord, measured from leading edge
x_c	Fraction of chord for field point on blade surface
x_h	Hub radius, fraction of tip radius
x_R	Fraction of radius, measured from axis of rotation
x_R	Radial coordinate for field point on blade surface
$Y_T(x_c)$	Nondimensional thickness offset maximum $Y_T = 0.5$
Z	Number of blades
α	Angular variable in chordwise direction
$\alpha(x_c, x_R)$	Component of derivative of surface coordinate
$\beta = \tan^{-1}\frac{J(1-w_x)}{x_R \pi}$	Advance angle of blade section
$\Gamma(x_R)$	Circulation distribution
$\gamma(x_c, x_R)$	Chordwise component of disturbance velocity difference across blade section
$\gamma^*(x_c)$	Chordwise velocity difference scaled to give unit magnitude when integrated across the chord
ϵ	Error bound. Increment to pitch angle when radial inflow exists
η	Integration variable along vortex filament
$\theta = \tan^{-1}\frac{-y}{z}$	Angular coordinate in cylindrical reference frame
$\theta_k = 2\pi(k-1)/Z$	Angular coordinate of blade reference line of k^{th} blade
$\theta_s(x_R)$	Skew angle, circumferential displacement of blade-section mid chord point from $y = 0$ plane
$\theta_m(x_c, x_R)$	Angular coordinate of point on blade-reference surface
$\Lambda = (\sigma, \gamma)$	Vorticity vector
$\mu(x_c, x_R)$	Normal component of disturbance velocity difference across blade section (source strength due to thickness)
(ξ_1, ξ_2, η)	Helical coordinates on pitch reference surface
ρ	Fluid density
$\sigma(x_c, x_R)$	Component of disturbance velocity difference across blade section
σ_s	Surface area
ϕ	Potential function for perturbation velocity, polar coordinate for field point
$\phi_P(x_R) = \tan^{-1}\frac{(P/D)}{\pi x_R}$	Pitch angle of blade reference surface, measured on cylinder of radius r
$\phi_g(x_R)$	Geometric pitch angle
$\psi(x_c)$	Radius of streamline on blade surface
ω	Angular variable in radial direction

INTRODUCTION

The design of an open marine propulsor is a complex process, involving structural and hydrodynamic considerations (1, 2). For the hydrodynamic considerations during most of the preliminary design process, approximate models of the lifting surfaces are employed, e.g., the lifting-line model (3, 4) for powering considerations, and two-dimensional flow over equivalent blade sections for cavitation performance. More sophisticated models of the lifting surfaces are used for predicting fluctuating loads (5) and some cavitation predictions (6). These approximate models have been acceptable *during the preliminary design process* and provide a basis for choice of the maximum diameter, advance coefficient and radial variations of chord, skew-angle, rake, thickness, and circulation distribution. The chordwise variation in load has usually been selected during this preliminary stage and is often based on cavitation and propulsion considerations.

For the final stage of the design, the meanline distribution and radial pitch variation are determined corresponding to the selections for load and geometry already available. To derive a geometry which accurately produces the specified load distributions, a lifting-surface model of the blades is required.

Several procedures already exist for performing lifting-surface calculations for wide-bladed open marine propulsors. In particular, two different approaches to the analysis for blades with arbitrary locations in space have been presented by Kerwin (7) and McMahon (8). Kerwin's numerical analysis procedure is based on three fundamental assumptions: (1) that the continuous loading distribution on the nonplanar blade surface can be adequately approximated by a multitude of discrete straight lines of constant-vortex strength and that the source distribution arising from the thickness distribution can be similarly approximated, (2) that the minimum required spacing between lattice elements along the chordline is $\Delta\theta = 2$ degrees, and (3) that the resulting meanline shape for a given chordwise load is similar to the two-dimensional shape for the same chordwise load. The *first two assumptions are not acceptable for very narrow blades*; for a blade with a 20 degree pitch angle at the 0.9

radius and a chord to diameter ratio of 0.05, the 2 degree spacing equals increments of about 1/3 chord length. The last assumption permits calculations to be performed using only a few points along the chord and the two-dimensional shape is fitted to the data at these points. The resulting computer code is relatively quick running and produces a geometry which, in practice, has an overall speed and powering performance generally within a few percent or so of the predicted values, with a general tendency to produce a greater thrust than predicted. The procedure of McMahon employs continuous distributions for the loading and thickness functions and calculates the meanline from the induced velocity. Consequently, data at more chordwise points are required to define the pitch and meanline distributions. The resulting computer code is lengthy to run but has shown remarkably different meanline shapes from the two-dimensional one at the hub and tip region of the blade where the meanlines can be s-shaped (8). Two models were constructed and experimentally evaluated to provide data on the relative cavitation and propulsion performance of designs having the same input specifications but final geometry according to the Kerwin and McMahon procedures. Some inconsistencies occurred in the experimental measurements but the thrust was closer to the predicted value and the operating point centered in the cavitation bucket for the model designed by the McMahon method. Hence, the determination of specific meanline and pitch distributions, instead of fitting the two-dimensional meanline, is considered to be a superior procedure when the design is based on a narrow range of permissible operating conditions and the delay of cavitation is critical.

Because the numerical-analysis procedure employed by McMahon results in lengthy computer runs and Kerwin's procedure is not acceptable for narrow blades, alternative numerical-analysis schemes are investigated in this paper. In addition, a detailed description of the flow field across the blade surface was desired as input into boundary-layer calculations. Two different numerical analysis schemes are described, each involving an expansion of the singular kernel about the singular point. Both approaches employ integration of the specified thickness slope and load distribution over the reference blade in the radial direction first and the remaining chordwise integration then takes the form of the velocity component corresponding to two-dimensional flow modified by the presence of an induction factor in the integral. Regular integration techniques are employed for the other blades and the shed vortex sheet. The induced velocity components are appropriately combined and integrated to obtain meanline shapes.

The present investigation describes the real-fluid flow about a rotating system of lifting surfaces having both loading and thickness. Several approximations are made. The first of these is the mathematical model for which potential flow equations are employed and the solution to first-order in thickness-to-chord ratio, camber-to-chord ratio and difference in pitch and flow angles derived. Comparisons with experimental results for other lifting-surface configurations lead to confidence in this linearized approximation. In addition to this mathematical model, further approximations occur in the numerical analysis. Confidence in the numerical analysis procedures is justified by comparison with analytical solutions or experimental results. That is, results are sought from some discretized numerical-analysis procedures involving N by M approximations, which have converged to within some specified tolerance, ϵ, of the real or analytical value of the quantity investigated. Mathematically this may be stated

$$|f(x,y) - f_{N,M}(x,y)| < \epsilon$$

$$\text{for } \begin{cases} (x,y) \text{ on the surface } S \\ N \geq N_0 \\ M \geq M_0 \end{cases}$$

where $f_{N,M}$ = the approximate calculation of a particular quantity f

S = a region of the surface of interest

N_0, M_0 = minimum numbers of the discrete approximations for which the computed results are within ϵ of the values for f

For rotating lifting surfaces, neither measured nor analytical solutions exist for details of the flow field on the blade. Hence, comparisons will be made with other procedures. It is assumed that numerical solutions which employ increasingly greater pointwise definition of the input variable without change in computed values have converged and that the solution has converged when a smooth curve can be drawn through point values in both the chordwise and radial directions. These assumptions are believed to be necessary but not sufficient for convergence.

In the following sections, the mathematical model of the flow field on the blade surface is first reviewed and numerical-analysis techniques for evaluating both regular and singular integrals are described. A FORTRAN computer code is discussed and sample calculations using this code are presented. From example calculations, it is found that greater accuracy in the integral evaluations is required for the determination of smooth pressure distribution curves than for the shape of the meanline and the pitch distributions. The choice of a particular chordwise loading distribution is shown to have an effect on the meanline shape and the pressure distribution. The effects of rake and skew are shown to be important on both pressure distribution and meanline shape. A particular thickness function has hardly any effect on pitch or meanline but a significant effect on pressure distribution.

MATHEMATICAL MODEL — THICK LIFTING BLADE

The mathematical model of a system of rotating lifting surfaces advancing in an unbounded irrotational flow field with an inviscid fluid has been developed on a formal mathematical basis by Brockett (9). A reformulation of that analysis in terms of non-dimensional surface coordinates is presented herein for completeness. The propulsor is assumed to be adequately represented by the blades alone, i.e., neither the hub nor fillet from the blades to the hub is included in the blade specification. The onset flow is assumed to be directed along the axis of rotation but a new feature included herein is that it may have a small radial component. Overall geometry notation generally follows the definitions given in Reference 10.

Coordinate systems are constructed with the same orientation as in Reference 9, and in particular, the helical coordinate system (ξ_1, ξ_2, r) rotating with the blades is shown in Figure 1. Unit base vectors in a right-handed Cartesian reference frame are the customary (i, j, k) where i is along the x axis and is positive pointing aft, j is along the y axis and k is along the z axis which is generally along the reference blade. Unit vectors along the helical coordinates are

$$e_1 = \sin\phi_p \, i + \cos\phi_p \, e_\theta \tag{1}$$

$$e_2 = -\cos\phi_p \, i + \sin\phi_p \, e_\theta \tag{2}$$

$$e_r = \sin\theta \, j + \cos\theta \, k \tag{3}$$

where

$$e_\theta = \cos\theta \, j - \sin\theta \, k \tag{4}$$

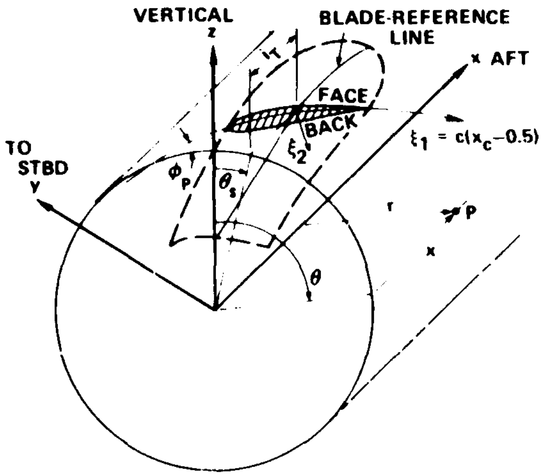

Fig. 1 Lifting-surface geometry

The blade surface is given by

$$\xi_2 = F(\xi_1, r) \tag{5}$$

$$= E_c(\xi_1, r) \pm E_T(\xi_1, r) \tag{6}$$

where

E_c is the meanline shape, and

E_T is the thickness shape

In the analysis, it is convenient to change the variables of integration to (x_c, x_R) instead of (ξ_1, r), where

$$\left.\begin{aligned} \xi_1 &= c\,(x_c - 0.5) \\ r &= D\,x_R/2 \\ c &= \text{chordlength at radius } r \\ \text{and} \quad D &= \text{maximum rotor diameter} \end{aligned}\right\} \tag{7}$$

The position vector of a point on the blade surface described by Equation (5) is

$$s = D\left\{\left[\frac{i_T}{D} + \frac{c}{D}(x_c - 0.5)\sin\phi_P - \frac{F}{D}\cos\phi_P\right] i + \frac{x_R}{2}\,e_r(\theta)\right\} \tag{8}$$

and a normal, directed out from the blade surface, is (9, 11)

$$N = \pm\,\frac{\partial s}{\partial x_c} \times \frac{\partial s}{\partial x_R} \tag{9}$$

where the plus sign is used for the suction side of the blade and the negative sign for the pressure side of the blade After some effort it can be shown that

$$N = \pm\,\frac{D^2}{2}\left\{\frac{c}{D}\,e_2 - \frac{\partial F/D}{\partial x_c}\,e_1 + N_R\,e_r\right\} \tag{10}$$

where

$$N_R = -2\,\frac{c}{D}\,\frac{\partial E/D}{\partial x_R} + 2\,(x_c - 0.5)\,\frac{d\,c/D}{d\,x_R}\,\frac{\partial E/D}{\partial x_c}$$

$$+\,2\,\frac{d\,i_T/D}{d\,x_R}\left[\frac{c}{D}\cos\phi_P + \frac{\partial E/D}{\partial x_c}\sin\phi_P\right]$$

$$+\,2\left[\left(\frac{c}{D}\right)^2 (x_c - 0.5) + \frac{E}{D}\,\frac{\partial E/D}{\partial x_c}\right]$$

$$\cdot\left[\frac{d\,P/D}{d\,x_R}\,\frac{\cos^2\phi_P}{\pi\,x_R} - \frac{\sin\phi_P\cos\phi_P}{x_R}\right]$$

$$-\left[x_R\,\frac{d\,\theta_s}{d\,x_R} - 2\,\frac{\frac{c}{D}(x_c - 0.5)\cos\phi_P + \frac{E}{D}\sin\phi_P}{x_R}\right]$$

$$\cdot\left[\frac{c}{D}\sin\phi_P - \frac{\partial E/D}{\partial x_c}\cos\phi_P\right]$$

The normal to the blade reference surface, $\xi_2 = 0$, $0 \le x_c \le 1$, $x_h \le x_R \le 1$ is

$$N_o = \pm\,\frac{D^2}{2}\,\frac{c}{D}\left[e_2 + N_{R_o}\,e_r(\theta_o)\right] \tag{11}$$

where

$$N_{R_o} = 2\,\frac{d\,i_T/D}{d\,x_R}\cos\phi_P + 2\left(\frac{c}{D}\right)(x_c - 0.5)$$

$$\cdot\,\frac{d\,P/D}{d\,x_R}\,\frac{\cos^2\phi_P}{\pi\,x_R} - x_R\,\frac{d\,\theta_s}{d\,x_R}\sin\phi_P$$

N_{R_o}, the radial component of the normal, is zero for a constant-pitch blade which is neither raked nor skewed In Equations (10) and (11)

i_T = the total rake

P = the pitch of the blade

ϕ_P = the pitch angle, $\phi_P = \tan^{-1}(P/(\pi x_R D))$

θ = the angular position of a point on the blade surface, a function of both x_c and x_R

$$= 2\,\frac{b-1}{Z}\,\pi + \theta_s + 2\left[\frac{c}{D}(x_c - 0.5)\cos\phi_P + \frac{F}{D}\sin\phi_P\right]\Big/ x_R$$

θ_s = the skew angle, a function of x_R

and

$$\theta_o = 2\,\frac{b-1}{Z}\,\pi + \theta_s + 2\,\frac{c}{D}\,(x_c - 0.5)\cos\phi_P / x_R$$

In the derivation of the expressions for numerical analysis the reference surface (F = 0) is often employed Generally no specific mention will be made of differences between variables on the blade surface and on the reference surface

In a coordinate system rotating with the blades the fluid velocity may be taken to be the sum of the undisturbed velocity and a component due to the disturbance of the blades [illegible] (12)

$q_{\theta} = $ [illegible] (13)

where V = the constant reference speed

$1-w_x$ = the wake fraction multiple to obtain the local axisymmetric speed[1]

w_R = the radial component of inflow, fraction of the reference speed

n = the rotational speed, revolutions per unit time, and

v = the velocity component due to the presence of the blades

If β_p is the pitch angle and β is the advance angle

[illegible]

[illegible] (14)

[illegible]

The difference of Equations (12) and (10) gives

[illegible]

$$s_h = s_{o_h} + D\left\{\left[\frac{i_T}{D} + \frac{c}{D}(x_c - 0.5)\sin\phi_p\right] [illegible] + \frac{x_R}{2} c_r(\theta_o)\right\} \qquad (25)$$

Hence Equation (23) can be reduced to an integral over only one side of the blade surfaces and shed vortex sheets

$$\underline{v}(\underline{r}) = \frac{1}{4\pi}\sum_{h=1}^{Z}\int_0^1 d\,x_c \int_{x_h}^1 d\,x_R$$

$$\cdot\left[(\underline{N}^+ \cdot \underline{v}^+ + \underline{N}^- \cdot \underline{v}^-)\frac{\underline{r} - \underline{s}_{o_h}}{\left|\underline{r} - \underline{s}_{o_h}\right|^3}\right.$$

$$\left. + (\underline{N}^+ \times \underline{v}^+ + \underline{N}^- \times \underline{v}^-) \times \frac{\underline{r} - \underline{s}_{o_h}}{\left|\underline{r} - \underline{s}_{o_h}\right|^3}\right]$$

$$+ \frac{1}{4\pi}\sum_{h=1}^{Z}\int_{x_h}^1 dx_R \int_0^\infty d\eta\, \frac{dx_c}{d\eta}\,[\underline{N}^+ \times (\underline{v}^+ - \underline{v}^-)]$$

$$\times \frac{\underline{r} - \underline{s}_{w_h}}{\left|\underline{r} - \underline{s}_{w_h}\right|^3} \qquad (26)$$

where

$$\frac{s_{w_h}}{D} = \left(\frac{x_c}{D} + [illegible] \sin\phi_p\right) [illegible]$$

$$+ \frac{x_R}{2} [illegible] (\theta_e + [illegible] \cos\phi_p\, x_R + \theta_h)$$

[illegible]

$$+ \frac{[illegible]}{D} [illegible] (1\ 0)$$

As the field point $\underline{r}$ approaches a point $\underline{r}_o$ (x_{c_o}, x_{R_o}) on the surface of the blade, Equation (23) or (26) becomes singular. If a small region about this point is excluded from the surface S and the limit of the integral taken for $\underline{r} \to \underline{r}_o$ with the excluded area tending to zero, there results (see Reference 9):

$$[illegible] = \frac{1}{4\pi}\sum_{h=1}^{Z} ⨍_0^1 dx_c ⨍_{x_h}^1 dx_R$$

$$\cdot\left[(\underline{N}^+ \cdot \underline{v}^+ + \underline{N}^- \cdot \underline{v}^-)\frac{\underline{r}_o - \underline{s}_{o_h}}{\left|\underline{r}_o - \underline{s}_{o_h}\right|^3}\right.$$

$$\left. + (\underline{N}^+ \times \underline{v}^+ + \underline{N}^- \times \underline{v}^-) \times \frac{\underline{r}_o - \underline{s}_{o_h}}{\left|\underline{r}_o - \underline{s}_{o_h}\right|^3}\right]$$

$$+ [illegible] \qquad (27)$$

$$+ \frac{1}{4\pi}\sum_{h=1}^{Z}\int_{x_h}^1 dx_R \int_0^\infty d\eta\, \frac{dx_c}{d\eta} \qquad (27\ \text{cont.})$$

$$\cdot \frac{[\underline{N}^+ \times (\underline{v}^+ - \underline{v}^-)] \times (\underline{r}_o - \underline{s}_{w_h})}{\left|\underline{r}_o - \underline{s}_{w_h}\right|^3}$$

where the symbol $⨍$ means symmetry restrictions on the limiting region which excludes the singularity. For example (9), the region may be square, circular, or rectangular centered at $\underline{r}_o$. In the present application, the rectangular region $x_{c_o} - \epsilon < x_c < x_{c_o} + \epsilon$, $x_h < x_R < 1$ will be the shape of the excluded region. Then this principal value integral is defined

$$⨍_0^1 dx_c \int_{x_h}^1 dx_R\, K = \lim_{\epsilon \to 0}\left[\int_0^{x_{c_o}-\epsilon} dx_c \int_{x_h}^1 dx_R\, K + \int_{x_{c_o}+\epsilon}^1 dx_c \int_{x_h}^1 dx_R\, K\right] \qquad [illegible]$$

The assumption

$$\lim_{\underline{r} \to \underline{r}_o^+} [\underline{v}(\underline{r})] = \underline{v}^+(\underline{r}_o) \qquad [illegible]$$

(i.e., that the velocity defined in the field does approach the value on the boundary) leads to the following expression for the average velocity component on the blade surface

$$\underline{v}\left(x_{c_o}, x_{R_o}\right) = \frac{1}{2}\left[\underline{v}^+\left(x_{c_o}, x_{R_o}\right) + \underline{v}^-\left(x_{c_o}, x_{R_o}\right)\right] \qquad (30)$$

$$= \underline{v}_I + \underline{v}_I$$

$$= u\underline{e}_1 + v\underline{e}_2 + w\underline{e}_r$$

$$= \sum_{h=1}^{Z} ⨍_0^1 dx_c \int_{x_h}^1 dx_R\, K\left(x_{c_o}, x_{R_o}, x_c, x_R\right) + \underline{v}_w \qquad (31)$$

where the singular kernel is

$$K\left(x_{c_o}, x_{R_o}, x_c, x_R\right) = \frac{1}{4\pi}\left[(\underline{N}^+ \cdot \underline{v}^+ + \underline{N}^- \cdot \underline{v}^-)\frac{\underline{r}_o - \underline{s}_{o_h}}{\left|\underline{r}_o - \underline{s}_{o_h}\right|^3} + (\underline{N}^+ \times \underline{v}^+ + \underline{N}^- \times \underline{v}^-) \times \frac{\underline{r}_o - \underline{s}_{o_h}}{\left|\underline{r}_o - \underline{s}_{o_h}\right|^3}\right]$$

and the velocity induced by the shed vortex sheet is

[illegible]

[illegible] the strength of the sources [illegible] the strength of the vortex [illegible]

[illegible] of the blades and along the [illegible] a value for the [illegible] that the blade [illegible]

[illegible] (34)

Now [illegible] equation can be constructed for a coordinate [illegible] rotating with the blade (9) and the pressure [illegible] determined by

[illegible] (35)

[illegible] (36)

Let

[illegible] (37)

Then to first order

$$\gamma = \frac{p^- - p^+}{\rho V \sqrt{(1 - w_x)^2 + \left(\frac{\pi x_R}{J_v}\right)^2} \cos(\phi_p - \beta)} \quad (38)$$

$$= \frac{V}{2} \frac{\Delta C_p}{\sqrt{(1 - w_x)^2 + \left(\frac{\pi x_R}{J_v}\right)^2} \cos(\phi_p - \beta)} \quad (39)$$

and from Equation (20)

$$\mu = D^2 V \sqrt{(1 - w_x)^2 + \left(\frac{\pi x_R}{J_v}\right)^2} \cos(\phi_p - \beta) \frac{\partial F_T / D}{\partial x_c} \quad (40)$$

where

$$\Delta C_p = (p^- - p^+)/(\rho V^2/2) \quad (41)$$

It remains to determine σ. Now, in general

[illegible] (42)

and the value of σ can be determined by setting the divergence of the right hand side equal to zero. However, this results in a differential equation to be solved for σ. A more direct procedure is to express the perturbation velocity vector as the gradient of a potential

[illegible] (43)

where

[illegible] (44)

Thus

[illegible] (45)

and

[illegible] (46)

For [illegible]

[illegible] (47)

It is convenient to define

[illegible] (48)

where $\Gamma(x_R)$ is the bound circulation ($\phi^+ - \phi^-$ at the trailing edge and points beyond) and γ^* has unit magnitude when integrated across the chord. Let the nondimensional circulation G be

$$G = \frac{\Gamma}{\pi D V} \quad (49)$$

Then

$$\gamma = \pi V \frac{G(x_R)\,\gamma^*(x_c)}{c/D} \quad (50)$$

and

$$A \equiv \frac{N_o^+ \times \langle v \rangle}{2\pi D^2 V} = \frac{N_o^+}{4\pi D^2 V} \times \nabla \left[\pi V D G(x_R) \int_0^{x_c} \gamma^* \, dx_c \right] \quad (51)$$

[illegible] strength of the vortex distribution is explic[illegible] the integration to determine the average in[illegible] parts of the blade surface can be undertaken.

[illegible] field on the blade is [illegible] determined and the [illegible] integrating the slope

$$[illegible] \int [illegible] \, dx \qquad (66)$$

[illegible] Equation [illegible] the meanline offset for the term with [illegible] component can be directly com[illegible] consists of an angle of attack term due to gradient [illegible] the rake and skew terms and a parabolic arc meanline [illegible] gradients of the pitch.

[illegible] approximation for the non-linear speed [illegible] in the chordwise direction is [illegible]

$$\frac{q_s}{V} = \frac{\sqrt{[illegible] + \left(\frac{\pi x_R}{J_s}\right)^2 + [illegible]}}{\sqrt{1 + \left(\frac{d[illegible]}{dx}\right)^2}} \qquad (67)$$

Hence

$$\left(\frac{q}{V}\right)^2 = \left(\frac{q_s}{V}\right)^2 + \left(w_R e_r \cdot \hat{e} + \frac{v}{V} \cdot \hat{e}\right)^2 \qquad (68)$$

where $\hat{e}$ is the unit vector in the $N_o^* \times e_1$ direction (nearly the radial direction over much of the blade)

$$\hat{e} = \frac{N_o^* \times e_1}{|N_o^* \times e_1|} = \frac{e_r - N_{R_o} e_2}{\sqrt{1 + N_{R_o}^2}} \qquad (69)$$

NUMERICAL ANALYSIS PROCEDURE

[illegible]

[illegible]

The linearized integrand F for integration over the blade reference surface then becomes in the general form (where a, b and c depend on the particular case of loading or thickness)

$$F(x_c, x_{c_0}) = \sum_{i=1}^{3} \int_{x_h}^{1} dx_R \qquad (100)$$

$$\cdot \frac{\left[(x_R - x_{R_0}) a_i + (x_{c_0} - x_c) b_i\right] c_i}{\left[A(x_R - x_{R_0})^2 + B(x_R - x_{R_0})(x_{c_0} - x_c) + \left(\frac{c}{D}\right)^2 (x_{c_0} - x_c)^2\right]^{3/2}}$$

$$= \sum_{i=1}^{3} (a_i D_1 + b_i D_2)\, c_i$$

where

$$D_1 = \int_{x_h}^{1} \frac{(x_{c_0} - x_c)(x_R - x_{R_0})\, dx_R}{\left[\rho(x_R - x_{R_0}, x_{c_0} - x_c)\right]^3}$$

$$= \frac{2}{\left[4A\left(\frac{c}{D}\right)^2 - B^2\right]} \qquad (101)$$

$$\cdot \left[\frac{B(1 - x_{R_0}) + 2\left(\frac{c}{D}\right)^2 (x_{c_0} - x_c)}{\sqrt{A(1 - x_{R_0})^2 + B(1 - x_{R_0})(x_{c_0} - x_c) + \left(\frac{c}{D}\right)^2 (x_{c_0} - x_c)^2}} - \frac{B(x_h - x_{R_0}) + 2\left(\frac{c}{D}\right)^2 (x_{c_0} - x_c)}{\sqrt{A(x_h - x_{R_0})^2 + B(x_h - x_{R_0})(x_{c_0} - x_c) + \left(\frac{c}{D}\right)^2 (x_{c_0} - x_c)^2}}\right]$$

[illegible]

At the singular point $x_c = x_{c_0}$

$$F(x_{c_0}, x_{R_0}, x_{c_0}) = 4 \frac{\sum_{i=1}^{3} (\ldots a_i B + \ldots b_i A)\, c_i}{\sqrt{A}\left[4A\left(\frac{c}{D}\right)^2 - B^2\right]} \qquad (103)$$

This known value at the singular point allows a straightforward analysis procedure to be undertaken using the procedures previously described.

Some convergence problems near the leading and trailing edges and over much of the surface for narrow blades (maximum c/D ≈ 0.05) have been resolved by computing the linearized form of F (Equation 100) over the entire blade and adding a correction term which is the difference between the actual integrand and this *linear approximation*. This option has been included in the computer program and is defined as "linear approximation-plus-difference." When conventional integration techniques are used everywhere except at the singular point, where Equation (103) is required, the procedure is defined as "direct."

For the trailing-vortex sheet, a regular integration can be performed since no singular points occur on the sheet. The strength of the vorticity is given by Equation (59) and the induced velocity field is given by

$$\frac{v}{V} = \frac{1}{4}\int_0^1 \left(-\frac{dG}{dx_R}\right) \sum_{h=1}^{Z} W(r_o, x_R, \theta_h)\, dx_R \qquad (104)$$

where

$$W(r_o, x_R, \theta_h) = \int_0^\infty e_1 \times \frac{\frac{r_o}{D} - \frac{s_{w_h}}{D}}{\left|\frac{r_o}{D} - \frac{s_{w_h}}{D}\right|^3}\, d\eta \qquad (105)$$

For a given value of ... the number of intervals N ... constant increment ...

$$\Delta\chi = \frac{\chi_N}{N}$$

for which the increment ... between successive points is

$$\Delta\ldots$$

$$(\ldots) \frac{\eta_1}{4N} \quad (10)$$

and the increment in angular variable θ between successive points is

$$\Delta\theta_i = 2\Delta\chi \cos\phi_P\, x_R$$

$$(\ldots)\cos\phi_P\,\eta_1 \ldots x_R\, 4N^2 \ldots \quad (11)$$

from which

$$\Delta\theta_1 = \frac{\eta_1}{4N}\,\frac{2\cos\phi_P}{x_R}$$

and

$$\Delta\theta_N = \frac{4N-1}{4N^2}\,\eta_1\,\frac{2\cos\phi_P}{x_R} = (4N-1)\,\Delta\theta_1$$

Generally $\eta_1 = \eta_2$ and the equal increments of χ, η are used for integration with $N = 2\eta_1$ double intervals. A value of $\eta_1 = 10$ has been satisfactory to date. When the distance between points becomes small, special fine point spacing in η is employed to insure convergence. Accuracy of calculations was determined by comparison with analytical results for the tangential velocity component due to a circular arc vortex filament, the axial velocity component at the origin for a general helical filament, all velocity components for a straight line vortex, and induction factors (17) for general helical filaments. At individual points of this comparison for filaments accuracy to the third decimal point was found with the selected parameters and an overall accuracy of the nondimensional induced velocity component of the sheet to one or two units in the fourth decimal point was found.

$$\ldots \left[\left(\frac{x_{\ldots}}{D} - \frac{x_{te}}{D}\right) \ldots\right] \ldots$$

$$\frac{\cos\phi_P}{2}\left[x_R - x_{R_0}\cos\left(\theta_{te} + \theta_h - \phi\right.\right.$$

$$\left.\left. + 2\eta\,\frac{\cos\phi_P}{x_R}\right)\right] \ldots + \left[\left(\frac{x_{\ldots}}{D} - \frac{x_{te}}{D}\right.\right.$$

$$\left.\eta\sin\phi_P\right)\cos\phi_P\sin\left(\theta_{te} + \theta_h - \phi\right.$$

$$\left. + 2\eta\,\frac{\cos\phi_P}{x_R}\right) + \frac{\sin\phi_P}{2}\left(x_{R_0}\right.$$

$$\left. x_R\cos\left(\theta_{te} + \theta_h - \phi + 2\eta\,\frac{\cos\phi_P}{x_R}\right)\right]e_{\ldots}$$

$$+\left[\left(\frac{x_{\ldots}}{D} - \frac{x_{te}}{D} - \eta\sin\phi_P\right)\cos\phi_P\cos\left(\theta_{te}\right.\right.$$

$$\left. + \theta_h - \phi + 2\eta\,\frac{\cos\phi_P}{x_R}\right) + \frac{\sin\phi_P}{2}\,x_R\sin\left(\theta_{te}\right.$$

$$\left.\left. + \theta_h - \phi + 2\eta\,\frac{\cos\phi_P}{x_R}\right)\right]e_r(\phi) \quad (9b)$$

In order to perform calculations the form of s^* and non-dimensional thickness must also be specified. A general family of loading functions has been selected (18) with the property that they have zero values at the leading and trailing edges and resemble conventional NACA loading functions (19). The zero values at the ends are necessary for accurate fit with a sine series trigonometric interpolation polynomial. For loading distributions which approximate the NACA a-series meanlines the following chordwise form is used:

[illegible]

[illegible] K [illegible] taken sufficiently large to make the load distribution in the leading edge region nearly rectangular. A previous investigation (18) of this loading function for K = 8 and [illegible] demonstrated that it was an acceptable approximation of the NACA a = 0.8 meanline (see Figure 2). Some trial chordwise loading functions were selected to [illegible]

[illegible] K [illegible] (13)

Each selected load distribution must be integrated across the chord and scaled to produce a unit value for the integral.

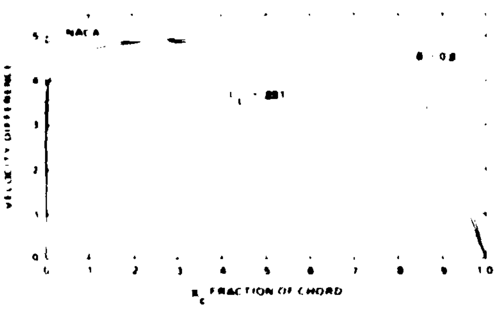

Fig. [illegible] Load distribution

The thickness offset is assumed in the form

$$\frac{t_T}{D} = \frac{t(x_R)}{D} \cdot \frac{1}{[illegible]}(x_R) \cdot Y_T(x) \qquad (14)$$

where the chordwise distribution $Y_T(x)$ remains the same from root to tip; only the maximum value changes with radius. This is true for current propulsor designs. Specific examples of the thickness function included in the computer code are the NACA 4 and 5 digit sections (19), the NACA 16 section (20), an elliptic nose quartic tail section similar to that described in Reference 21, and an approximate NACA a = 0 Modified section. All have been analytically defined.

Computer Code — Convergence and Run Time

The complexity of the numerical analysis [illegible] error estimates are difficult to establish. No [illegible] exist for which analytic integration may be performed. Comparisons do not usually evaluate the general [illegible]. The procedure selected to evaluate convergence was to vary the number of intervals in the radial direction NR and the number of intervals in the chordwise direction NX. Results from some radial and chordwise points were interpolated from the calculations. Computed values of the pitch and camber at selected radii are shown in Table I together with a similar variation of data calculated according to the procedure described in Reference 7 for the same propeller which is similar to NSRDC Model 4498. Computer central processing time is for computations at 13 radii between the extreme radii listed and is in seconds for the Burroughs 7700 High Speed Computer. Current charges are 3 cents per CPU second resulting in a maximum charge of about $40. All procedures presented produce about equally satisfactory results with about only one percent difference in pitch [illegible] and for values about the same as found for Kerwin's numerical analysis. The computed pitch, however, is a few percent less than computed by Kerwin's method. Since unpublished experience at DTNSRDC to date has been that Kerwin's procedure produces designs that are generally slightly overpitched, perhaps some improvement in performance may be expected using the present method.

Predictions of the pitch and camber by the two procedures developed for computing the induced velocity field on the blade surface which contains the field point ("direct" and "approximate plus difference") are shown in Table I to be nearly the same. However, it has been found that overall the "approximate plus difference" procedure is preferable when dense chordwise spacing is chosen (e.g., NX = 19) or narrow blades (maximum c/D = 0.05) are involved. In these situations, the "direct" procedure produces locally erratic values of the induced velocity because of the decreased spacing between adjacent lines of integration with a corresponding lack of accuracy in the numerical integrations for the resulting near-singular integrals. This effect is illustrated in Figure 3 which shows values of one of the helical components of the average induced velocity at the 0.946 radius of the reference blade. This velocity component is due to only loading on the blade itself; the effects of thickness, the other blades and the shed vortex sheet are not included. All data shown in subsequent figures have been computed by the "approximate plus difference" procedure although only the pressure distribution near the leading edge in the tip region of the blade was significantly different between the two procedures.

Overall run time varies with number of points, number of blades, and blade width. Since computer usage charges are so low, the 181 x 19 array size is recommended. For a narrow blade, the linear "approximation plus difference" procedure is recommended and the run time may increase by a few hundred seconds because of special care taken with the shed vortex sheet calculations. Computer execution time for Kerwin's program is unknown for the Burroughs 7700 high speed computer but is estimated to be about 150 seconds for data calculations at 4 chordwise points at 8 radial stations. For the results shown in Table I, data are computed at 13 radial stations with either 8, 11, or 17 chordwise points depending on input data specification.

Further details of the geometry of this example are given in Table II. Radial variables are titled according to the symbols suggested in Reference 10.

Table I
Effect of Parameters on Pitch, Camber and Computer Run Time

COMPUTATIONAL PROCEDURE

x_R	[illegible] Direct	18T x 10 Direct	18T x 13 Direct	9T x 19 Direct	18T x 19 Direct	9T x 19 Approx + Diff	18T x 19 Approx + Diff	Kerwin Computation: $\Delta\theta$ [illegible] M [illegible]	Kerwin Computation: $\Delta\theta$ [illegible] M [illegible]
					PITCH DIAMETER				
								1.580	1.603
[illegible]	1.49[illegible]	1.498	1.51	1.5[illegible]	1.538	1.539	1.540	1.576	
[illegible]	1.46[illegible]	1.46[illegible]	1.4[illegible]	1.48[illegible]	1.48[illegible]	1.48	1.488	1.511	1.52[illegible]
	[illegible]64	[illegible]64	[illegible]	[illegible]	[illegible]	[illegible]	[illegible]	1.292	1.296
[illegible]	[illegible]84	[illegible]184	[illegible]189	1.194	1.193	1.193	1.193	1.213	
[illegible]	1.038	1.038	1.040	1.043	1.042	1.04[illegible]	1.042	1.065	1.070
[illegible]	0.88[illegible]	0.88[illegible]	0.882	0.884	0.883	0.883	0.883	0.894	
								0.890	0.88[illegible]
					CAMBER CHORD				
								0.0266	0.025[illegible]
[illegible]	[illegible]	0.030[illegible]	0.0315	0.0320	0.032[illegible]	0.0323	0.0324	0.0268	
[illegible]	[illegible]	0.0368	0.036[illegible]	0.0368	0.0368	0.0369	0.0369	0.0356	0.0351
	[illegible]	[illegible]	0.0293	0.0298	0.0295	0.0295	0.0295	0.0301	0.0294
	[illegible]	[illegible]	0.025[illegible]	0.025[illegible]	0.0258	0.0254	0.025[illegible]	0.0257	
[illegible]	[illegible]	0.0189	0.0189	0.0188	0.0189	0.0188	0.0188	0.0181	0.0180
[illegible]	[illegible]	0.0124	0.012[illegible]	0.012[illegible]	0.0123	0.0123	0.0122	0.0122	
								0.0120	0.0113
[illegible]	[illegible]	420	600	[illegible]	1085	[illegible]85	1135	N A	N A

Fig. 3 Helical velocity component [illegible]

DISCUSSION OF EXAMPLE COMPUTATIONS

In this section, the consequences of choices the designer might make both for overall geometry and for the chordwise variation of the thickness distribution and loading distribution are examined. Some common variations in the location of the blade mid-chord line are investigated to determine the effects of overall geometry on pitch, camber, pressure distribution, and second-order performance coefficients. The variations are unskewed, skewed and warped (23) blades with other input specifications the same. Skewed blades have blade-sections displaced along the pitch helix and warped blades have blade sections displaced circumferentially in the plane at $x = 0$.

Input quantities and selected output are shown in Table II for a warped blade similar to NSRDC Model 4498 (and one similar to the example of Reference 7). For an unskewed blade, the column labeled TETS, the skew angle θ_s, would be zero, and for a skewed blade the column labeled RAKE/D, the total rake i_T/D, would be equal to $P \cdot \theta_s/(2\pi D)$. In Figure 4, the computed pitch and camber ratios are shown for these various overall geometries with all other input the same as in Table II. In Figure 5 the effects of the chordwise load distribution and chordwise thickness function on pitch and camber are shown. The effect of rake and skew on pitch and camber follows known trends (7, 24). The effect of thickness distribution on pitch and camber is negligible and the effect of elliptic loading is to reduce the pitch and increase the camber, as would be the case in two dimensional flow at the ideal angle for a given lift coefficient. In Figure 6, the pitch and camber change is shown for another modification of the warped blade. Since a large change occurs in the pitch from the input specification (Table II) to the computed values (Figure 4), computations were performed with the singularities distributed on the blade reference surface at a pitch taken from Figure 4. This change in pitch places the singularities nearer the final blade surface. To have uniformity in the calculations, the pitch angle of the shed vortex sheet was taken as β, the advance angle of the shed vortex sheet. (In Figure 4, the shed vortex sheet was taken to be at the input pitch, which is β_i, the pitch angle derived from the solution of a straight radial lifting line representing each blade.) The change in pitch angle of the shed vortex wake from β_i to β produces a slight increase of pitch near the hub (compare data in Figures 4 and 6). A change in the pitch of the blade reference surface to the values shown by the dashed curve in Figure 4 produces a significant reduction in computed pitch and a compensating increase in camber near the root, with negligible change in either pitch or camber from about $x_R = 0.5$ to the tip. Hence the orientation of the free vortex sheet and blade reference surface have significant effects on the pitch and camber values only near the hub.

Table II
DEFINITION OF DESIGN EXAMPLE
Sample Data from Computer Code

4498 EXAMPLE LOADING AND THICKNESS, 5 BLADES - SEPT 80

CIRCULATION COEFFICIENTS

N	G(N)
1	0.029020
2	0.002010
3	-0.002830
4	-0.000540
5	0.000081
6	0.000081

DIAMETER = DP 0.3048 M ADVCY V/(ND) = 0.8080 NPB = Z = 5

INPUT DATA

XR	CH/DP	PP/DP	RAKT/DP	TETS	TMAX/CH
0.20000	0.16500	1.16270	0.00000	0.00000	0.24000
0.25000	0.19700	1.19530	0.00000	0.07854	0.19800
0.30000	0.22600	1.22790	0.00000	0.15708	0.15610
0.40000	0.27500	1.25980	0.00000	0.31416	0.10680
0.50000	0.31200	1.25570	0.00000	0.47124	0.07690
0.60000	0.33700	1.21600	0.00000	0.62832	0.05650
0.70000	0.34700	1.15960	0.00000	0.78540	0.04210
0.80000	0.33400	1.09870	0.00000	0.94248	0.03160
0.90000	0.28000	1.03570	0.00000	1.09956	0.02460
0.95000	0.24000	1.00660	0.00000	1.17810	0.02330
1.00000	0.00000	0.97350	0.00000	1.25664	0.02460

4498 EXAMPLE LOADING AND THICKNESS, 5 BLADES - SEPT 80

XR	CH/DP	(CH/DP)'	PP/DP	(PP/DP)'	RAKT/DP	TETS	(TETS)'	TMAX/CH	(TMAX/DP)'	VE/V
0.20000	0.16500	0.62731	1.16270	0.63950	0.00000	0.00000	1.57080	0.24000	-0.82618	1.00000
0.20648	0.16882	0.62982	1.16659	0.64013	0.00000	0.00955	1.57080	0.23490	-0.82679	1.00000
0.22412	0.18020	0.63075	1.17870	0.64825	0.00000	0.03799	1.57080	0.21999	-0.83583	1.00000
0.25359	0.19936	0.65792	1.19776	0.69126	0.00000	0.08618	1.57080	0.19600	-0.87251	1.00000
0.29320	0.22510	0.60910	1.22416	0.60026	0.00000	0.14700	1.57080	0.16097	-0.77784	1.00000
0.34200	0.25127	0.46041	1.24736	0.53807	0.00000	0.22644	1.57080	0.13002	-0.49779	1.00000
0.40000	0.27500	0.39203	1.25990	0.17505	0.00000	0.31416	1.57080	0.10683	-0.34834	1.00000
0.46319	0.29926	0.36617	1.26143	-0.08327	0.00000	0.41362	1.57080	0.08667	-0.28746	1.00000
0.53036	0.32119	0.27019	1.24678	-0.34858	0.00000	0.51971	1.57080	0.06970	-0.21751	1.00000
0.60000	0.33700	0.17799	1.21600	-0.51613	0.00000	0.62832	1.57080	0.05650	-0.16700	1.00000
0.66966	0.34573	0.06936	1.17761	-0.58232	0.00000	0.73743	1.57080	0.04606	-0.13522	1.00000
0.73681	0.34596	-0.07546	1.13751	-0.65699	0.00000	0.84322	1.57080	0.03775	-0.11189	1.00000
0.80000	0.33400	-0.33023	1.09870	-0.62592	0.00000	0.94248	1.57080	0.03160	-0.08871	1.00000
0.85712	0.30705	-0.59158	1.06273	-0.61250	0.00000	1.03220	1.57080	0.02699	-0.06529	1.00000
0.90642	0.27597	-0.82309	1.03169	-0.62442	0.00000	1.10966	1.57080	0.02632	-0.04245	1.00000
0.94641	0.24651	-1.18469	1.00693	-0.67063	0.00000	1.17266	1.57080	0.02330	-0.00309	1.00000
0.97560	0.18500	-3.11163	0.98052	-0.62210	0.00000	1.21875	1.57080	0.02375	0.02963	1.00000
0.99392	0.10000	-7.95654	0.97720	-0.67256	0.00000	1.24709	1.57080	0.02457	0.03849	1.00000
1.00000	0.00000	-99.59900	0.97350	-0.62258	0.00000	1.25666	1.57080	0.02660	0.03802	1.00000

4498 EXAMPLE LOADING AND THICKNESS, 5 BLADES - SEPT 80

ELLIPSE WITH AIRFOIL TAIL AND CHORDWISE LOAD

XC	YT	DY/DANG	SIANG	COSANG	ZO U/V	GAM +	GAMINT	[illegible]
0.000000	0.000000	0.500000	0.000000	1.000000	1.300224	0.000000	0.000000	[illegible]
0.007596	0.086824	0.492404	0.173648	0.984808	1.005011	0.912003	0.005181	[illegible]
0.030154	0.171010	0.469846	0.342020	0.939693	1.004562	0.992665	0.027568	[illegible]
0.066987	0.250000	0.433013	0.500000	0.866025	1.005799	1.040099	0.066678	[illegible]
0.116970	0.321394	0.383022	0.642788	0.766044	1.005703	1.076103	0.117961	[illegible]
0.178606	0.383022	0.321394	0.766044	0.642788	1.007070	1.097916	0.186685	[illegible]
0.250000	0.433013	0.250000	0.866025	0.500000	1.008799	1.114007	0.263966	[illegible]
0.328990	0.469846	0.171010	0.939693	0.342020	1.012850	1.120317	0.352110	[illegible]
0.413176	0.492404	0.086824	0.984808	0.173648	1.017101	1.132910	0.447616	[illegible]
0.500000	0.500000	-0.000000	1.000000	-0.000000	1.029601	1.135109	0.545966	[illegible]
0.586824	0.492202	-0.091111	0.984808	-0.173648	1.055502	1.135109	0.644652	[illegible]
0.671010	0.467219	-0.148511	0.939693	-0.342020	1.095197	1.135109	0.740081	[illegible]
0.750000	0.421900	-0.322500	0.866025	-0.500000	1.092086	1.103570	0.829166	[illegible]
0.821394	0.356026	-0.462016	0.766044	-0.642788	0.998106	0.969260	0.903256	[illegible]
0.883022	0.269637	-0.561366	0.642788	-0.766044	0.721556	0.712637	0.956960	[illegible]
0.933013	0.176665	-0.526602	0.500000	-0.866025	0.229560	0.453126	0.986277	[illegible]
0.969846	0.091629	-0.410961	0.342020	-0.939693	-0.610899	0.216717	0.996676	[illegible]
0.992404	0.031655	-0.263726	0.173648	-0.984808	-1.501501	0.056755	0.999761	[illegible]
1.000000	0.010090	-0.161576	0.000000	-1.000000	-2.014221	0.000000	1.000000	[illegible]

TOTAL ANGLE = 2.456 DEG

Table II

SOME COMPUTED VARIABLES

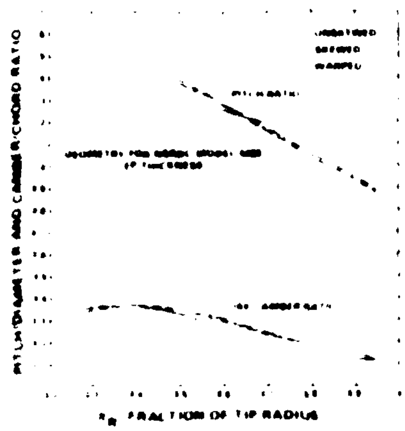

Fig. 4 Effect of skew and rake on pitch and camber values

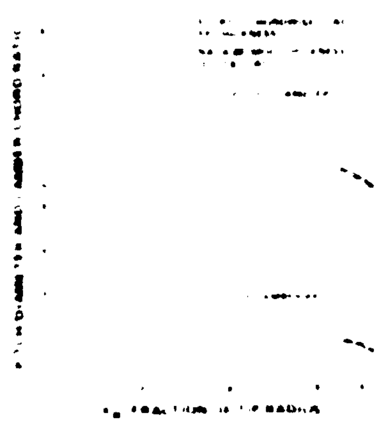

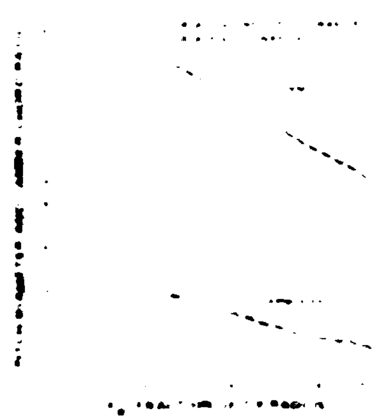

In Figure [illegible] blade pressure coefficient distribution on the warped, skewed and unskewed blades are shown for three radii: one near the hub, one near mid-span and one near the tip. The major difference in pressure distribution occurs near the hub where the warped blades have greater suction on both sides of the blade and hence a greater tendency to cavitate when the local pressure reaches the vapor pressure.

In Figure 8 the meanline shapes for these blades at the same three radii are shown. The greatest change in meanline shape [illegible] at the root [illegible]

In Figure [illegible] the [illegible] pressure distribution [illegible] Equations [illegible] and [illegible] and meanline shape are shown [illegible] [illegible] for the same variation [illegible] thickness distributions shown in Figure [illegible]

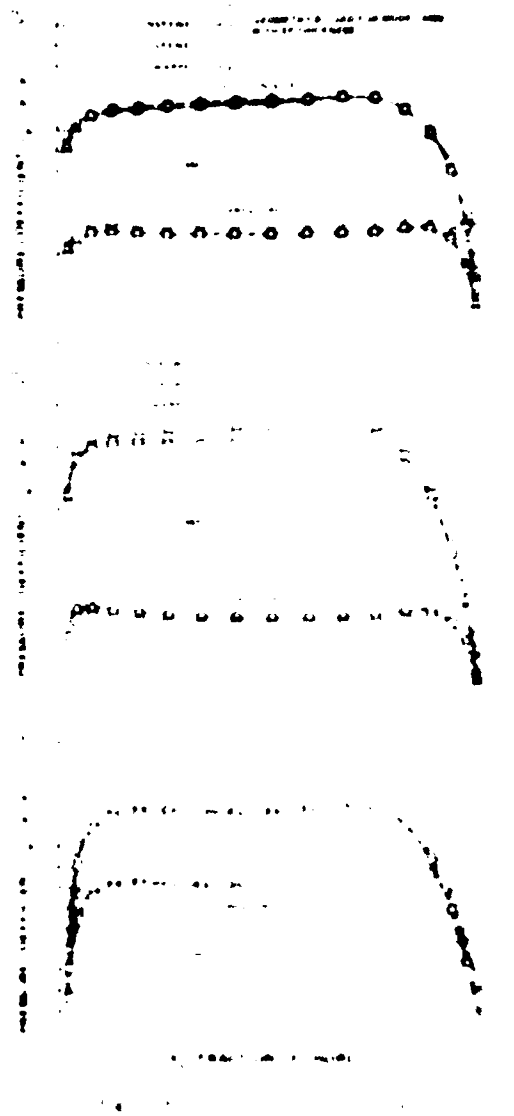

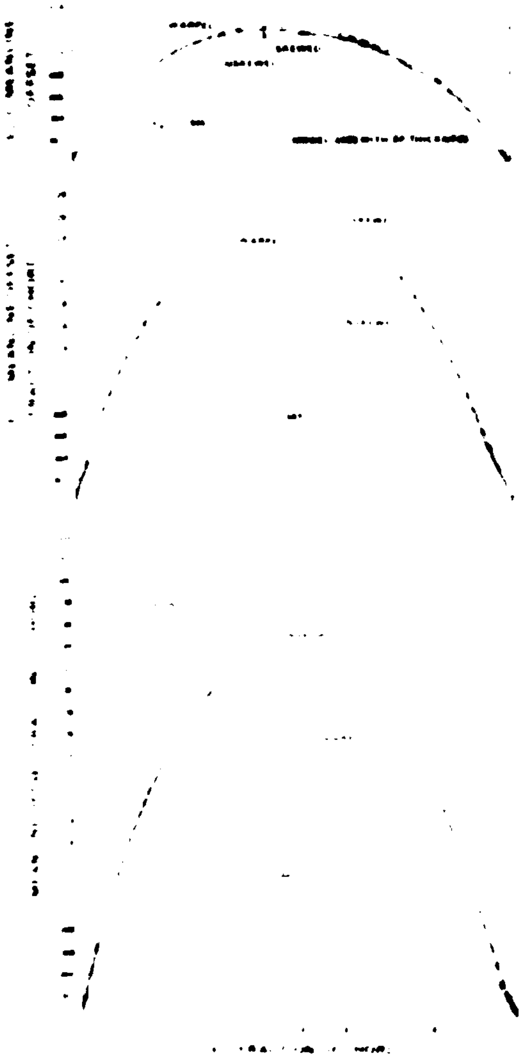

modifications. The performance coefficients computed according to the lifting line model and first order linear lifting surface model (C_T [illegible] in Equations (76) and (78)) and ΔC_p from Equation (74) are nearly identical. The nonlinear performance coefficients (C_T [illegible] in Equations (76) and (81)) and C_p from Equation (80) for a blade with only loading (C_p [illegible]) are increased a few percent relative to the lifting line values. The addition of thickness and skew or warp changes the pressure distribution and meanline slope and increases the values by another few percent, eventually producing values of C_T and C_p which are more than ten percent greater than predicted by the lifting line model. [illegible] The pressure distribution and [illegible] nonlinear [illegible] order [illegible] have been [illegible] theory. [illegible] the calculated [illegible] with these [illegible] are [illegible]. Experimental evaluation is required to confirm the predictions. Predictions given in Table III should be interpreted as possible trends in the actual performance. The present lifting line model [illegible] propeller design [illegible] assumes a straight radial [illegible] constant [illegible] to represent the blade [illegible] an acceptable [illegible] especially [illegible] with skewed or warped blades. [illegible] the majority of [illegible] have [illegible] with a few percent [illegible] significant differences have also [illegible] lifting [illegible] performance [illegible] should be [illegible]

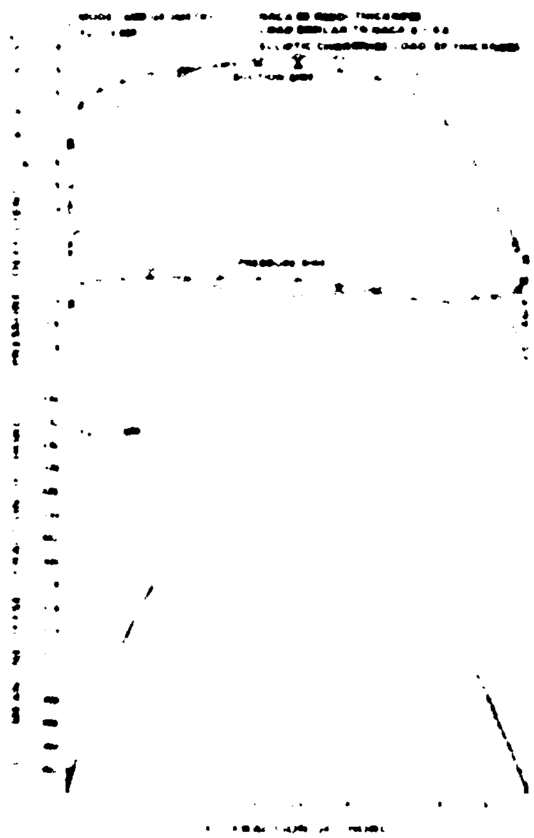

6. P. van Oossanen, "Calculation of Performance and Cavitation Characteristics of Propellers Including Effects of Non-uniform Flow and Viscosity," Netherlands Ship Model Basin Publication No. 457 (1974).

7. J.E. Kerwin, "Computer Techniques for Propeller Blade Section Design," International Shipbuilding Progress, Vol. 20, No. 227, July 1973; also MIT Dept. of Ocean Engineering, October 1975.

8. J.F. McMahon, "LETSUR — A Computer Program for Determining Hydrodynamic Pitch, Meanline Shape, and Pressure Distribution for Marine Propellers," DTNSRDC/SPD-731-01, 1976 (unpublished).

9. Terry Brockett, "Propeller Perturbation Problems," NSRDC Report 3880, October, 1972.

10. H. Lackenby, editor, "International Towing Tank Conference Standard Symbols 1976," British Ship Research Association Technical Memorandum No. 500, May, 1976.

11. A.P. Wills, Vector Analysis with an Introduction to Tensor Analysis, Dover Publications, Inc., 1931.

12. H.B. Phillips, Vector Analysis, Wiley, 1933.

13. J. Weber, "The Calculation of the Pressure Distribution on the Surface of Cambered Wings and the Design of Wings with Given Pressure Distribution," Aeronautical Research Council R&M 3026, 1955.

14. I.S. Sokolnikoff and R.M. Redheffer, Mathematics of Physics and Modern Engineering, McGraw-Hill, 1958.

15. H. Glauert, The Elements of Aerofoil and Airscrew Theory, Cambridge, 1926.

16. Terry Brockett, "A Subroutine for Evaluation of One-Dimensional Singular Integrals (SINGINT)," Defence Research Establishment Atlantic, Technical Memorandum 79 F, December, 1979.

17. W.B. Morgan, "Propeller Induction Factors," DTMB Report 1183, November, 1957.

18. Terry Brockett, "The Design of Two-Dimensional Profiles from a Specified Surface Speed Distribution Part 1 — Meanline at Ideal Angle of Attack," Defence Research Establishment Atlantic, Technical Memorandum 79 G, December, 1979.

19. I.H. Abbott and A.E. von Doenhoff, Theory of Wing Sections, Dover, 1959.

20. W.F. Lindsey, et al., "Aerodynamic Characteristics of 24 NACA 16-Series Airfoils at Mach Numbers between 0.3 and 0.8," NACA TN 1546, September 1948.

21. W.P. Rader, "Cavitation of Propeller Blade Sections," Admiralty Experimental Works, Haslar, Report 22/54, March, 1954.

22. Terry Brockett, "Minimum Pressure Envelopes for Modified NACA-66 Sections with NACA a = 0.8 Camber and BuShips Type I and Type II Sections," DTMB Report 1780, February, 1966.

23. J.F. Nelka, "Experimental Evaluations of a Series of Skewed Propellers with Forward Rake," NSRDC Report 4113, July, 1974.

24. R. A. Cumming, et al, "Highly Skewed Propellers," Trans. SNAME, Vol 80, 1972

25. T. T. Huang, et al, "Stern Boundary-Layer Flow on Axisymmetric Bodies," Twelfth Symposium on Naval Hydrodynamics, National Academy of Sciences, Wash. D.C., 1978.

26. Damon E. Cummings, "Numerical Prediction of Propeller Characteristics," Journal of Ship Research, Vol 17, No. 1, March, 1973.

27. Nancy Groves, "An Integral Prediction Method for Three-Dimensional Turbulent Boundary Layers on Rotating Blades," Paper presented at "Propellers '81 Symposium," SNAME, May, 1981.

APPENDIX – STREAMLINE COORDINATE SYSTEM

It is often convenient to have an orthogonal coordinate system on the surface of the blade. In particular, for performing boundary-layer computations, an orthogonal coordinate system with one variable along the streamlines reduces the number of terms in the governing equations. To determine the differential equation of the streamline path, let

$$x_R = \psi(x_c) \tag{120}$$

be the radius of the streamlines as a function of the chordwise coordinate x_c. Then

$$s^*(x_c) = s(x_c, \psi(x_c)) \tag{121}$$

is the position vector of the streamlines on the blade surface. Hence a tangent to the streamline is

$$t_\psi = \frac{ds^*}{dx_c} = \left(\frac{\partial s}{\partial x_c}\right)_{x_R=\psi} + \left(\frac{\partial s}{\partial x_R}\right)_{x_R=\psi} \cdot \frac{d\psi}{dx_R}$$

$$= D\left[\frac{c}{D} e_1 + \left(\alpha e_1 + \frac{N_0^* \times e_1}{D^2 \frac{c}{D}}\right)\frac{d\psi}{dx_R}\right] \tag{122}$$

$$= D\left[\left(\frac{c}{D} + \alpha \frac{d\psi}{dx_c}\right) e_1 + \frac{1}{2}\sqrt{1+N_{R_0}^2}\,\frac{d\psi}{dx_c}\,\hat{e}\right]$$

For this tangent vector to be parallel to the velocity vector on the surface, the vector cross product, $t_\psi \times q$, must be zero. Hence, for the velocity on the blade surface given by

$$\frac{q}{V} = \frac{q_\infty}{V} + \frac{v}{V}$$

$$= \frac{U}{V} e_1 + \frac{W}{V}\,\hat{e} \tag{123}$$

the cross product is

$$\frac{t_\psi}{D} \times \frac{q}{V} = \left\{\left(\frac{c}{D} + \alpha \frac{d\psi}{dx_c}\right) e_1 + \frac{\sqrt{1+N_{R_0}^2}}{2}\,\frac{d\psi}{dx_c}\,\hat{e}\right\} \times \left\{\frac{U}{V} e_1 + \frac{W}{V}\,\hat{e}\right\}$$

$$\left\{\frac{1}{2}\sqrt{1+N_{R_0}^2}\,\frac{d\psi}{dx_c}\,\frac{U}{V} + \left(\frac{c}{D} + \alpha \frac{d\psi}{dx_c}\right)\frac{W}{V}\right\},$$

For this cross product to be zero, the slope of the streamline is

$$\frac{d\psi}{dx_c} = \frac{\frac{c}{D}\,\frac{W}{V}}{\frac{1}{2}\sqrt{1+N_{R_0}^2}\,\frac{U}{V} - \alpha\,\frac{W}{V}} \tag{124}$$

For lines along the surface which are normal to the streamlines, let

$$x_c = \kappa(x_R) \tag{125}$$

be the chordwise position as a function of radius. Then a vector on the blade surface tangent to this line is

$$t_n = \frac{ds(\kappa(x_R), x_R)}{dx_R}$$

$$= \left(\frac{\partial s}{\partial x_c}\right)_{x_c=\kappa} \frac{d\kappa}{dx_R} + \left(\frac{\partial s}{\partial x_R}\right)_{x_c=\kappa} \tag{126}$$

$$= D\left[\frac{c}{D} e_1 \frac{d\kappa}{dx_R} + \alpha e_1 + \frac{1}{2}\sqrt{1+N_{R_0}^2}\,\hat{e}\right]$$

The condition to be satisfied is that t_n be perpendicular to the velocity vector, or

$$\frac{t_n}{D} \cdot \frac{q}{V} = 0 \tag{127}$$

$$= \frac{U}{V}\left(\frac{c}{D}\,\frac{d\kappa}{dx_R} + \alpha\right) + \frac{1}{2}\sqrt{1+N_{R_0}^2}\,\frac{W}{V} \tag{128}$$

Thus the slope of lines on the surface which are normal to the streamline is

$$\frac{d\kappa}{dx_R} = -\frac{\frac{1}{2}\sqrt{1+N_{R_0}^2}\,\frac{W}{V} + \alpha\,\frac{U}{V}}{\frac{c}{D}\,\frac{U}{V}} \tag{129}$$

One now has differential equations to determine an orthogonal network over the blade surface. The differential arc length along the streamlines is

$$ds = \left\{\left(\frac{\partial s}{\partial x_c}\right)_{x_R=\psi} + \left(\frac{\partial s}{\partial x_R}\right)_{x_R=\psi} \frac{d\psi}{dx_c}\right\} dx_c \tag{130}$$

Since

$$ds = |ds| = h_1\,dx_c \tag{131}$$

then

$$h_1 = \left| \left(\frac{\partial s}{\partial x_c}\right)_{x_R = \psi} + \left(\frac{\partial s}{\partial x_R}\right)_{x_R = \psi} \frac{d\psi}{dx_c} \right|$$

or

$$\frac{h_1}{D} = \left\{ \left(\frac{s}{D} + \alpha \frac{d\psi}{dx_c}\right)^2 + \frac{1 + N_{R_o}^2}{4} \left(\frac{d\psi}{dx_c}\right)^2 \right\}^{1/2} \tag{132}$$

Similarly the differential arc length along the orthogonal surface coordinate is

$$ds = \left| \left(\frac{\partial s}{\partial x_c}\right)_{x_c = \kappa} \frac{d\kappa}{dx_R} + \left(\frac{\partial s}{\partial x_R}\right)_{x_c = \kappa} \right| dx_R \tag{133}$$

$$= h_2 \, dx_R \tag{134}$$

where

$$\frac{h_2}{D} = \left\{ \left(\frac{s}{D} \frac{d\kappa}{dx_R} + \alpha\right)^2 + \frac{1 + N_{R_o}^2}{4} \right\}^{1/2} \tag{135}$$

INITIAL DISTRIBUTION

Copies	
1	ARMY CHIEF OF RES & DIV
1	ARMY ENGR R&D LAB
2	CHONR
	1 Code 438
	1 LIB
1	NRL
[illegible]	ONR BOSTON
[illegible]	ONR CHICAGO
[illegible]	ONR LONDON, ENGLAND
2	USNA
	1 LIB
	1 Johnson
1	NAVPGSCOL LIB
1	NROTC & NAVADMINU, MIT
1	NADC
5	NOSC
	1 1311 LIB
	1 6005
	1 13111 LIB
	1 2501/Hoyt
	1 Nelson
1	NWC
[illegible]	NAVSEA
	1 SEA 032
	1 SEA 0321
	1 SEA 03D
	1 SEA 052
	1 SEA 052P
	SEA 0521
	[illegible] SEA 052[illegible]
	[illegible] SEA 052[illegible]
	[illegible] SEA 0525
	[illegible] SEA [illegible]
	SEA [illegible]
	SEA [illegible]

Copies	
	1 PMS 378
	1 PMS 380
	1 PMS 381
	[illegible] PMS 38[illegible]
	[illegible] PMS 389
	[illegible] PMS [illegible]
	[illegible] PMS [illegible]
	1 PMS 39[illegible]
	1 PMS 39[illegible]
	[illegible] PMS 399
	[illegible] PMS [illegible]
	[illegible] SEA [illegible]
	[illegible]
1	FAC [illegible]
[illegible]	MILITARY SEALIFT COMMAND [illegible]
[illegible]	NAVSHIPYD PTSMH
1	NAVSHIPYD PHILA
1	NAVSHIPYD NORVA
1	NAVSHIPYD CHASN
1	NAVSHIPYD LBEACH
1	NAVSHIPYD MARE
1	NAVSHIPYD PUGET
[illegible]	NAV[illegible]
[illegible]	[illegible]
	[illegible]
[illegible]	[illegible]
[illegible]	[illegible]
[illegible]	MARAD
	[illegible]
	[illegible]
	[illegible]
	[illegible]
	[illegible]

Copies	
1	MISSISSIPPI, ME DEPT/Fox
1	NOTRE DAME ENGR LIB
5	PENN STATE U/ARL 1 LIB 1 Parkin 1 Henderson 1 Gearhart 1 Thompson
[illegible]	PRINCETON/Mellor
[illegible]	RENSSELAER MATH DEPT
[illegible]	[illegible]

Copies	
1	ASNE
1	SNAME
1	AERO JET-GENERAL/LIB
1	ALLIS CHALMERS, YORK, PA
1	AVCO LYCOMING
1	BAKER MANUFACTURING
2	BATH IRON WORKS CORP 1 Hansen 1 FFG PROJECT OFFICE
1	BETHLEHEM STEEL SPARROWS
[illegible]	BIRD-JOHNSON CO 1 Case 1 Ridley 1 Norton
[illegible]	BOEING ADV AMR SYS [illegible]
[illegible]	BOLT BERANEK AND NEWMAN 1 Brown 1 Jackson
[illegible]	BREWER ENGR LAB
[illegible]	CAMBRIDGE ACOUS [illegible]
[illegible]	CALSPAN, INC [illegible]
[illegible]	DOUGLAS AIRCRAFT 1 TECH LIB 1 Smith
[illegible]	EXXON RES DIV 1 LIB 1 Fitzgerald
[illegible]	[illegible]
[illegible]	GEN DYN CONVAIR ASW-MARINE SCIENCE

Copies

3 GIBBS & COX
- 1 TECH LIB
- 1 Olson
- 1 CAPT Nelson

1 GRUMMAN AEROSPACE/Carl

3 HYDRONAUTICS
- 1 Etter
- 1 Scherer
- 1 LIB

3 HYDRODYNAMICS RESEARCH ASSOCIATES, INC.
- 1 Cox
- 1 Valentine
- 1 Nelka

1 INGALLS SHIPBLDG

1 INST FOR DEFENSE ANAL

1 LITTLETON R & ENGR CORP/Reed

1 LITTON INDUSTRIES

1 LOCKHEED/Waid

1 MARITECH, INC/Vassilopoulis

1 NATIONAL STEEL & SHIPBLDG

1 NEWPORT NEWS SHIPBLDG LIB

1 NIELSEN ENGR/Spangler

4 ORI, INC
- 1 Kim
- 1 Schneider
- 1 Williams
- 1 Kobayashi

1 HYDROMECHANICS, INC/Kaplin

1 NAR SPACE/Ujihara

1 PROPULSION DYNAMICS, INC

1 PROPULSION SYSTEMS, INC

Copies

1 SCIENCE APPLICATIONS, INC/Stern

1 GEORGE G. SHARP

1 SPERRY SYS MGMT LIB/Shapiro

2 SUN SHIPBLDG
- 1 LIB
- 1 Neilson

1 ROBERT TAGGART

1 TETRA TECH PASADENA/Chapkis

1 TRACOR

1 UA HAMILTON STANDARD/Cornell

CENTER DISTRIBUTION

Copies	Code	Name
1	11	Ellsworth
1	1102.1	Nakonechny
1	15	Morgan
1	1509	Powell
1	152	Lin
1	1521	Day
1	1522	Wilson
1	1522	Dobay
1	1528	Reed
1	154	McCarthy
1	1543	Cumming
40	1544	Brockett
1	1544	Boswell
1	1544	Jessup
1	1544	Larimer
1	1552	Lee
1	1552	Libby
1	1556	Santore
1	1556	Coder
1	1556	Jeffers

CENTER DISTRIBUTION (Continued)

Copies	Code	Name
1	172	Krenzke
1	1720.6	Rockwell
1	19	Sevik
1	19	Strasberg
1	1903	Chertock
1	1962	Zaloumis
1	1962	Noonan
1	2814	Czyryca
10	5211.1	Reports Distribution
1	522.1	Library (C)
1	522.2	Library (A)

END

DATE

FILMED

11-81

DTIC